Cellular Physiology and Biochemistry

Cell Physiol Biochem 2018;47:1152-1166
DOI: 10.1159/000490210
Published online: June 18, 2018
Accepted: April 10, 2018

Original Paper

RA190, a Proteasome Subunit ADRM1 Inhibitor, Suppresses Intrahepatic Cholangiocarcinoma by Inducing NF-κB-Mediated Cell Apoptosis

Guang-Yang Yu[a] Xuan Wang[a] Su-Su Zheng[b] Xiao-Mei Gao[a] Qing-An Jia[a] Wen-Wei Zhu[a] Lu Lu[a] Hu-Liang Jia[a] Jin-Hong Chen[a] Qiong-Zhu Dong[a] Ming Lu[a] Lun-Xiu Qin[a]

[a]Department of General Surgery, Huashan Hospital & Cancer Metastasis Institute & Institutes of Biomedical Sciences, Fudan University, Shanghai, [b]Liver Cancer Institute, Fudan University, Shanghai, China

Key Words
Intrahepatic cholangiocarcinoma (ICC) • Proteasome subunit ADRM1 • RA190 • Apoptosis • PDX

Abstract
Background/Aims: Effective drug treatment for intrahepatic cholangiocarcinoma (ICC) is currently lacking. Therefore, there is an urgent need for new targets and new drugs that can prolong patient survival. Recently targeting the ubiquitin proteasome pathway has become an attractive anti-cancer strategy. In this study, we aimed to evaluate the therapeutic effect of and identify the potential mechanisms involved in targeting the proteasome subunit ADRM1 for ICC. ***Methods:*** The expression of ADRM1 and its prognostic value in ICC was analyzed using GEO and TCGA datasets, tumor tissues, and tumor tissue arrays. The effects of RA190 on the proliferation and survival of both established ICC cell lines and primary ICC cells were examined *in vitro*. Annexin V/propidium iodide staining, western blotting and immunohistochemical staining were performed. The *in vivo* anti-tumor effect of RA190 on ICC was validated in subcutaneous xenograft and patient-derived xenograft (PDX) models. ***Results:*** ADRM1 levels were significantly higher in ICC tissues than in normal bile duct tissues. ICC patients with high ADRM1 levels had worse overall survival (hazard ratio [HR] = 2.383, 95% confidence interval [CI] =1.357 to 4.188) and recurrence-free survival (HR = 1.710, 95% CI =1.045 to 2.796). ADRM1 knockdown significantly inhibited ICC growth *in vitro* and *in vivo*. The specific inhibitor RA190 targeting ADRM1 suppressed proliferation and reduced cell vitality of ICC cell lines and primary ICC cells significantly *in vitro*. Furthermore, RA190 significantly inhibited the proteasome by inactivating ADRM1, and the consequent accumulation of ADRM1 substrates decreased the activating levels of NF-κB to aggravate cell apoptosis. The therapeutic benefits of RA190 treatment were further demonstrated in both subcutaneous implantation and PDX models. ***Conclusions:*** Our findings indicate that up-regulated ADRM1 was involved in ICC

G.-Y. Yu, X. Wang and S.-S. Zheng contributed equally to this work.

Lun-Xiu Qin, MD, PhD, Prof & Director, Ming Lu, PhD and Qiong-Zhu Dong, PhD
Dept. of Gen. Surg., Huashan Hosp. & Cancer Metastasis Inst. & Inst. of Biomed. Sciences, Fudan Univ. 12 Urumqi Road (M), Shanghai 200040 (China)
E-Mail qinlx@fudan.edu.cn, luming@huashan.org.cn, qzhdong@fudan.edu.cn

progression and suggest the potential clinical application of ADRM1 inhibitors (e.g., RA190 and KDT-11) for ICC treatment.

Introduction

Intrahepatic cholangiocarcinoma (ICC) is the second most common primary liver cancer, with a 5-year survival rate less than 10% [1, 2]. The morbidity and mortality associated with ICC have increased worldwide in the past decade [2-4]. Since most ICC patients are diagnosed at an advanced stage and surgical resection remains the optimum curative option for ICC [5, 6], standardized treatment for these patients is currently inadequate [3, 5, 6]. Moreover, although gemcitabine and cisplatin are commonly used for inoperable ICC patients, they respond poorly to these chemotherapies [3, 7]. Therefore, it is essential to identify novel anti-tumor targets for ICC.

The 26S proteasome is a major component of the ubiquitin proteasome pathway, which is responsible for more than 80% of protein degradation in mammalian cells [8]. Since cancer cells require the ubiquitin proteasome pathway to permanently activate pro-tumor signal cascades, which promote cell cycle progression and prevents cell death resulting from aberrant stress [9], the use of inhibitors targeting the ubiquitin proteasome pathway is an attractive strategy for treating different cancers [10, 11]. Among these inhibitors, bortezomib is the first agent approved by the US Food and Drug Administration (FDA) for treating multiple myeloma [12].

Recently, a ubiquitin receptor ADRM1 [13] was found to be overexpressed in several malignancies [14-18]. However, the role of ADRM1 in these tumors has not been explored fully. Moreover, knockdown of ADRM1 suppresses tumor growth in different malignancies [15-18]. RA190, a novel specific inhibitor of ADRM1, was found to have a significant suppressive effect on multiple myeloma [14, 19]. However, the expression of ADRM1 in ICC and the effect and mechanism of action of targeting ADRM1 in ICC remain unclear.

In this study, we found that ADRM1 was elevated in ICC tissues compared with normal bile duct tissues; this was further validated by Gene Expression Omnibus (GEO) and The Cancer Genome Atlas (TCGA) datasets. In addition, ADRM1 overexpression predicted poor prognosis in ICC patients. Furthermore, targeting ADRM1 showed a significant therapeutic effect in ICC via inducing G_2-M cell cycle arrest and apoptosis both *in vitro* and *in vivo*. Together, we have provided proof-of-concept evidence that ADRM1 is a promising anti-tumor target in ICC. More importantly, targeting ADRM1 with RA190 may improve patient outcome in ICC.

Materials and Methods

Cell lines, culture, and reagents

Human ICC cell lines QBC939 (donated by Professor SG Wang at the Third Military Medical University, China) and RBE (purchased from the cell bank of Typical Culture preservation commission of the Chinese Academy of Sciences, Shanghai, China) were cultured in Dulbecco's modified Eagle's medium (HyClone, Logan, UT, USA), containing 10% fetal bovine serum (Gibco, Grand Island, New York, USA) and 1% penicillin-streptomycin solution, at 37 °C with 5% CO_2. RA190 was purchased from Xcess Biosciences (San Diego, CA, USA). For *in vitro* studies, RA190 stock solution (50 mM) was prepared in dimethyl sulfoxide (DMSO) and stored at -20 °C as small aliquots until needed. For *in vivo* studies, RA190 was dissolved in 15% 2-hydroxypropyl-β-cyclodextrin (HPBCD), and the solution was prepared freshly every week and stored in the dark at 4°C before use.

The primary ICC cells (ICC-1 and ICC-2) were established using freshly resected human ICC samples as previously described [20]. The primary cells were validated by their unique DNA short tandem repeat "fingerprints" matching that of the patient's tumor tissue.

Patients and specimens

In this study we used paraffin-embedded tissue samples from 102 consecutive ICC patients who underwent primary and potentially curative liver resections at the authors' institution from 2009 to 2014. Patients had not received any preoperative radiotherapy or chemotherapy. The clinicopathological and baseline demographic characteristics of the patients, including age, gender, tumor size, and tumor site, were retrospectively collected. Overall survival (OS) was calculated from the date of surgery to either the date of death or the last follow-up. Recurrence-free survival (RFS) was defined as the interval between the date of surgery and the first recurrence, or from the date of surgery to the date of last follow-up for patients without recurrence. Follow-up was terminated in December 2016. Ethical approval was obtained from the Research Ethics Committee, Fudan University, Shanghai, China and written informed consent regarding the use of tissue and data for scientific purposes was obtained from all participating patients.

Immunohistochemical staining of human ICC tissue arrays

Human ICC tumor tissue arrays were immunohistochemically stained with anti-ADRM1 antibody. The tissue array sections (5 μm) were dehydrated and subjected to peroxidase blocking. Primary antibodies were added and incubated at room temperature for 30 min using the DAKO AutoStainer and DakoCytomation EnVision+ System-HRP detection kit (Dakocytomation, Carpinteria, CA, USA). Slides were counterstained with hematoxylin. The stained slides were observed under microscopy, and images were acquired. Based on staining intensity, we classified the samples into four groups with increasing intensity from negative (Group 1) to strong (Group 4) for analysis [21].

GEO and TCGA databases

Data are publicly available from the GEO (accession number: GSE26566, https://www.ncbi.nlm.nih.gov/geo/query/acc.cgi?acc=GSE26566) [22] and TCGA (https://cancergenome.nih.gov/) databases.

RNA interference knockdown of ADRM1 and IκBα

Lentiviral infection was performed as described [23]. The shRNA sequences were: ADRM1 shRNA1: 5′-CCGGCCCTGACGACTGTGAGTTCAACTCGAGTTGAACTCACAGTCGTCAGGGTTTTTG-3′, shRNA2: 5′-CCGGCCGCGGATGAGATCCAGAATACTCGAGTATTCTGGATCTCATCCGCGGTTTTTG-3′; IκBα: shRNA: 5′-CCGGCTCCGAGACTTTCGAGGAAATCTCGAGATTTCCTCGAAAGTCTCGGAGTTTTTG-3′.

Cell viability assessment

RBE, QBC939, ICC-1, and ICC-2 cells were each seeded in 96-well plates with 1×10^3 cells per well in triplicate, and then treated with RA190 or DMSO for various time periods. Cell viability was detected by Cell Counting Kit-8 (Dojindo, Kumamoto, Japan) following the manufacturer's instructions.

Clonogenic assay

RBE and QBC939 cells (each 300/well) and ICC-1 and ICC-2 cells were each seeded in 6-well plates each 1000/well per well in triplicate and cultured for 12 days. The colonies were fixed with 4% paraformaldehyde and stained with crystal violet. Colonies with more than 30 cells were counted. Representative results of three independent experiments with similar trends are presented.

Real-time polymerase chain reaction analyses

Total RNA was isolated using Trizol reagent (Invitrogen, Carlsbad, CA, USA) according to the manufacturer's instructions and treated with RNase-free DNase. The reverse transcription reaction was performed using 2 μg total RNA per sample and the PrimerScript reverse transcription reagent kit (Takara, Shiga, Japan) according to the manufacturer's protocol. After reverse transcription, real-time polymerase chain reaction (PCR) was performed using Power SYBR Green PCR MasterMix (Applied Biosystems, Foster City, CA, USA) and the ABI 7900 thermocycler (Applied Biosystems) following the manufacturer's manual. The primer sequences are as follows: Human β-actin: forward 5′-TGACGTGGACATCCGCAAAG-3′, reverse 5′-CTGGAAGGTGGACAGCGAGG-3′; Human ADRM1: Forward 5′-CTGGCTGTGGCTCATGTTT-3′, reverse 5′-ACCCAAGACAGACCAGGATG-3′.

Propidium iodide staining and fluorescence-activated cell sorting analysis

Cells treated with RA190 or DMSO for various time periods were harvested and fixed in 70% ethanol at -20°C overnight, and stained with propidium iodide (PI, 36 μg/mL, Sigma, St. Louis, MO) containing RNase (10 μg/mL, Sigma) at 37°C for 30 min, then analyzed for apoptosis and cell cycle profile with CyAnTM ADP (Beckman Coulter, Fullerton, CA). Apoptosis was measured as the percentage of cells in the sub-G_1 population. Data were analyzed with ModFit LT software [24].

Annexin V -fluorescein isothiocyanate and PI staining and fluorescence-activated cell sorting analysis

Cells were treated with DMSO or RA190 for the indicated times. Then, cells were collected and stained with annexin V-fluorescein isothiocyanate (FITC) and PI using an annexin V-FITC apoptosis detection kit (BD Biosciences, San Jose, CA) followed by flow cytometric analysis. Data were analyzed with FlowJo 7.6 software [25].

Immunoblotting analysis

Cell lysates were prepared with cell lysis buffer (Beyotime, Haimen, China) and the protein concentration in the lysates was quantified using an enhanced BCA protein assay kit (Beyotime). Protein samples (50μg) were loaded for immunoblotting using antibodies against γ-H2AX, cleaved-PARP, PARP, cleaved-CASPAS3, PUMA (Cell Signaling Technology, Inc., Danvers, MA, USA), p-IκBα(S32) (Sangon Biotech, Shanghai, China), WEE1, p21, p27, ADRM1 and GAPDH (Abcam, Cambridge, MA, USA).

In vivo antitumor effect of RA190 on ICC

Five-week-old male athymic nude mice were purchased from Shanghai Experimental Animal Center (Shanghai, China). QBC939 cells were trypsinized, resuspended in phosphate-buffered saline, and subcutaneously implanted into the groin (5×10^6 cells per injection). The PDX mouse model was generated according to the previously reported protocol [26]. After 1 week, tumor- bearing mice were randomly divided into two groups (eight mice/group) and treated with RA190 or vehicle alone, twice a week for 4 weeks. Tumor size was measured weekly using vernier calipers. At the end of the study, the mice were killed and tumor tissues were collected, photographed, and weighed. Paraffin-embedded tissues were sectioned for immunohistochemistry of Ki-67 (Abcam), TUNEL assay (Promega, Madison, WI, USA), WEE1 (Abcam) and p-IκBα (Sangon Biotech). All procedures were performed in accordance with the National Institutes of Health Guide for the Care and Use of Laboratory Animals.

Statistical analysis

Data are presented as mean ± standard deviation. Student's *t* test was used for the comparison of parameters between two groups or two-way analysis of variance when comparing more than two groups. Survival was analyzed using the Kaplan–Meier method. A Cox proportional hazards model was used to calculate hazard ratio (HR) and the corresponding 95% confidence interval (CI) with adjustment for potential confounders. Statistical Program for Social Sciences software 17.0 (SPSS, Chicago, IL, USA) was used for statistical analyses.

Results

ADRM1 is overexpressed in human ICC tissue

First, we examined the expression of ADRM1 in 12 paired ICC tissues and normal bile duct tissues and found that the protein level of ADRM1 was increased in tumor tissues compared with paired normal bile duct tissues (Fig. 1A and 1B). Then the mRNA levels of ADRM1 were tested in 167 cases of ICC tissues and 12 cases of normal bile duct tissues from our institution. The results showed that ADRM1 mRNA levels were increased in ICC tissues compared with normal bile duct tissues (Fig. 1C). The up-regulation of ADRM1 in ICC was further validated in reported GEO (GSE26566) [22] and TCGA datasets (Fig. 1D and1E). These data indicate that ADRM1 is overexpressed at both mRNA and protein levels in human ICC tissues.

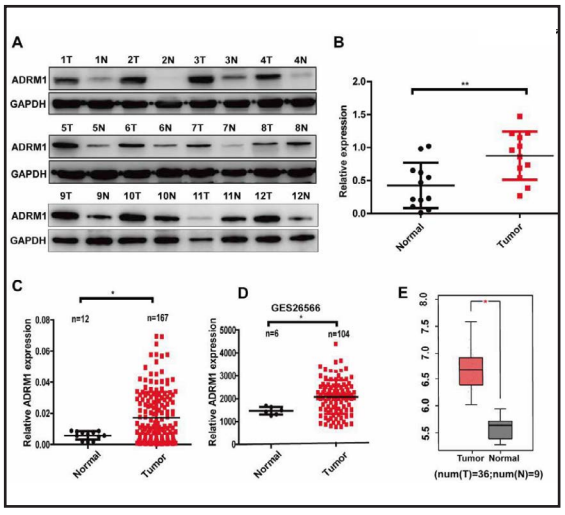

Fig. 1. The expression pattern of ADRM1 in ICC. (A) Immunoblotting analysis of the expression of ADRM1 in ICC tissues and normal bile duct tissues (n = 12). T, tumor; N, normal. (B) Quantification of ADRM1 expression in ICC tissues and normal bile duct tissues. The results of 12 pairs of tissues (tumor vs normal tissues) were analyzed. (C) Quantitative reverse transcription PCR analysis of ADRM1 mRNA levels in ICC tissues and normal bile duct tissues. (D) Relative mRNA expression of ADRM1 mRNA in ICC tissues and normal bile duct tissues in GSE26566. (E) Relative mRNA expression of ADRM1 in ICC tissues and normal bile duct tissues in TCGA dataset. *p <0.05, **p<0.01.

Overexpression of ADRM1 predicts poor prognosis of ICC

To investigate the prognostic value of ADRM1 for ICC, we further analyzed the pathological clinical characteristics of 102 ICC patients. These patients were divided into high-ADRM1 (strong or moderate intensity) or low-ADRM1 (weak or negative intensity) groups according to protein level (Fig. 2A and 2B). We found that ADRM1 levels in tumor tissues were significantly correlated with tumor size (Fig. 2C and Table 1) and that patients in the high-ADRM1 group had shorter OS and reduced RFS compared with those in the low-ADRM1 group (Fig. 2D). High expression of ADRM1 was associated with poor OS and RFS of ICC patients in univariable (OS: p = 0.003, HR = 2.383, 95% CI = 1.357 to 4.188; RFS: p = 0.033, HR = 1.710, 95% CI = 1.045 to 2.796) and multivariable (OS: p = 0.006, HR = 2.246, 95% CI = 1.259 to 4.006; RFS: p = 0.031, HR = 1.760, 95% CI = 1.054 to 2.939) survival analyses (Table 2). In the analysis of TCGA data, we found that ADRM1 overexpression also predicted poor prognosis of liver cancer (p = 0.00177), lung cancer (p = 0.0214), and renal cancer (p < 0.001) and glioblastoma (p = 0.0248) (for all online suppl. material, see www.karger.com/doi/10.1159/000490210, Suppl. Fig. 1). These results demonstrate that ADRM1 is overexpressed in human ICC and associated with reduced OS and RFS.

Table 1. Clinicopathological characteristics in ICC patients (n = 102). Abbreviations: HBsAg, hepatitis B surface antigen; AFP, alpha-fetoprotein; CA 19-9, carbohydrate antigen 19-9; ALT, alanine aminotransferase. †Fisher's exact test; chi-squared test for all other analyses

Clinicopathological Indexes		ADRM1		*P*
		Low	High	
Age (year)	< 61	18	31	0.770
	≥ 61	18	35	
Sex	Female	14	24	0.801
	Male	22	42	
HBsAg	Negative	22	44	0.575
	Positive	14	22	
Serum AFP (ng/mL)	< 20	35	58	0.154†
	≥ 20	1	8	
Serum CA 19-9, ng/mL	< 36	15	30	0.713
	≥ 36	21	36	
Serum ALT, U/L	< 40	24	46	0.753
	≥ 40	12	20	
Serum ALP, U/L	< 145	30	46	0.131
	≥ 145	6	20	
Serum CEA, μg/L	< 5	22	42	0.801
	≥ 5	14	24	
γGGT， U/L	< 60	18	30	0.660
	≥ 60	18	36	
Child-Pugh score	A	34	57	0.320†
	B	2	9	
Liver cirrhosis	No	29	56	0.578
	Yes	7	10	
Tumor number	Single	31	49	0.126†
	Multiple	5	17	
Microvascular/bile duct invas	No	26	49	0.825
	Yes	10	17	
Lymphatic metastasis	No	24	35	0.183
	Yes	12	31	
Tumor encapsulation	complete	2	10	0.206†
	none	34	56	
Tumor differentiation	poor	19	39	0.538
	moderate to well	17	27	

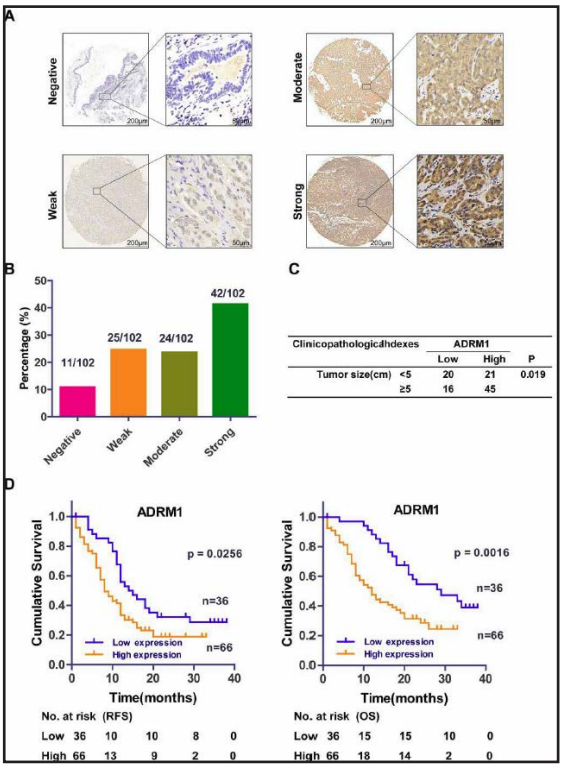

Fig. 2. Overexpression of ADRM1 correlated with poor prognosis of ICC patients. (A) Representative immunostaining images showing strong, moderate, weak and negative expression of ADRM1 (200× magnification). (B) Classification of samples according to staining intensity of ADRM1. (C) Correlation analysis of ADRM1 expression with tumor size. (D) Kaplan-Meier curves of RFS and OS rate of ICC patients stratified by ADRM1 expression.

ADRM1 silencing suppresses the growth of ICC cells in vitro and in vivo

ADRM1 overexpression in ICC suggests that it may be a useful therapeutic target. To validate this hypothesis, we knocked down ADRM1 in RBE and QBC939 cells using two shRNAs targeting two well-defined regions of ADRM1 (shA1 and shA2, respectively). The knockdown efficiency was validated by immunoblotting (Fig. 3A). ADRM1 knockdown significantly inhibited the proliferation of RBE and QBC939 cells (Fig. 3B). ADRM1 silencing also notably suppressed colony formation of these two cell lines (Fig. 3C). In addition, with regard to *in vitro* tumor formation ability, tumor growth in the shADRM1 group was significantly suppressed compared to the control group (Fig. 3D and 3E). These data indicate that ADRM1 is required for tumor growth of ICC.

Inhibition of ADRM1 by RA190 suppresses the proliferation of ICC cells in vitro

Recent studies have demonstrated that RA190 is an inhibitor of ADRM1. RA190 can covalently bind to ADRM1 in the 19S regulatory particle, resulting in inhibition of proteasome function and accumulation of higher-molecular weight polyubiquitylated proteins [14, 19]. Since ADRM1 also mediates the degradation of IκBα [27], we hypothesized

Table 2. Univariate and multivariate analyses of prognostic factors in ICC patients (n = 102). NOTE: Cox proportional hazards regression model. Abbreviations: HBsAg, hepatitis B surface antigen; AFP, alpha-fetoprotein; ALT, alanine aminotransferase; CA 19-9, carbohydrate antigen 19-9; HR, hazard ratio; CI, confidential interval

Variable	RFS		OS	
	HR(95%CI)	*P*	HR(95%CI)	*P*
Univariate analysis				
Age, year (≥61 versus < 61)	1.218(0.769-1.928)	0.400	1.250(0.758-2.601)	0.382
Sex (male versus female)	0.810(0.507-1.294)	0.378	0.809(0.488-1.342)	0.413
HBsAg (positive versus negative)	0.559(0.338-0.924)	**0.023**	0.411(0.232-0.729)	**0.002**
Serum AFP,ng/mL (≥20 versus < 20)	2.108(1.008-4.405)	**0.047**	1.829(0.868-3.856)	0.112
Serum CA 19-9, ng/mL (≥36 versus < 36)	1.637(1.019-2.631)	**0.042**	2.289(1.323-3.960)	**0.000**
Serum ALT, U/L (≥40 versus < 40)	1.237(0.759-2.015)	0.394	1.604(0.958-2.687)	0.073
Serum ALP, U/L (≥145versus < 145)	1.784(1.088-2.925)	**0.022**	2.159(1.283-3.633)	**0.004**
Serum CEA, μg/L (≥5 versus < 5)	1.561(0.980-2.484)	0.061	2.204(1.337-3.632)	**0.002**
γGGT, U/L (≥60versus < 60)	1.459(0.916-2.324)	0.111	2.289(1.349-3.884)	**0.002**
Child-Pugh score (A versus B)	1.324(0.658-2.665)	0.431	1.394(0.663-2.930)	0.381
Liver cirrhosis (no versus yes)	0.785(0.430-1.431)	0.429	0.837(0.436-1.607)	0.594
Tumor size, cm (≥5 versus < 5)	1.404(0.870-2.266)	0.164	1.798(1.054-3.068)	0.031
Tumor number (multiple versus single)	1.606(0.952-2.711)	0.076	1.701(0.983-2.943)	0.058
Vascular invasion (yes versus no)	1.387(0.841-2.288)	0.200	1.163(0.673-2.011)	0.588
Lymphatic metastasis (yes versus no)	1.969 (1.241-3.124)	**0.004**	3.069(1.840-5.120)	**0.000**
Tumor encapsulation (complete versus none)	0.642(0.295-1.401)	0.266	0.548(0.219-1.366)	0.197
Tumor differentiation (poor versus moderate to well)	1.598(0.994-2.568)	0.053	1.241(0.751-2.052)	0.400
ADRM1 (high versus low)	1.710(1.045-2.796)	**0.033**	2.383(1.357-4.188)	**0.003**
Multivariate analysis				
HBsAg (positive versus negative)	0.604(0.326-1.007)	0.053	0.483(0.267-0.871)	**0.016**
Serum CA 19-9, ng/mL (≥36 versus < 36)	1.510(0.903-2.525)	0.116	1.870(1.055-3.312)	**0.032**
Serum ALT, U/L (≥40 versus < 40)	1.069(0.638-1.792)	0.800	1.098(0.620-1.945)	0.748
Lymphatic metastasis (yes versus no)	1.698(1.028-2.807)	**0.039**	2.321(1.310-4.111)	**0.004**
Tumor size, cm (≥5 versus < 5)	1.018(0.599-1.731)	0.964	1.220(0.682-2.182)	0.503
ADRM1 (high versus low)	1.760(1.054-2.939)	**0.031**	2.246(1.259-4.006)	**0.006**

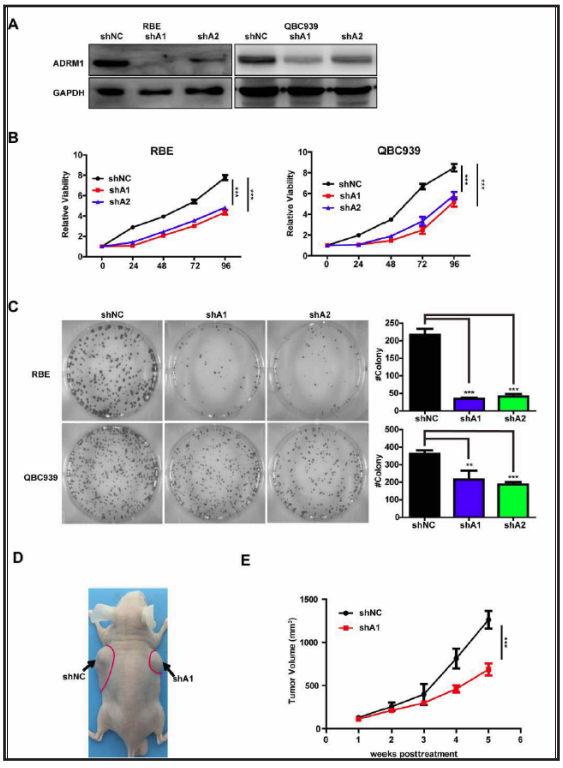

Fig. 3. The growth-suppressive effect of ADRM1 silencing on ICC cells in vitro and in vivo. (A) Knockdown efficiency was determined. Cells were subjected to immunoblotting analysis of the expression of ADRM1. (B) ADRM1 silencing by shRNA inhibited the proliferation of RBE and QBC939 cells. Cell proliferation was detected by cell counting kit-8 assay. (C) Silencing of ADRM1 suppressed colony formation of RBE and QBC939 cells. These results were representative of three independent experiments. (D-E) ADRM1 knockdown inhibited the growth of QBC939 cells in vivo. Representative image of xenograft tumor growth in vivo (D) and tumor growth curve (E). **p<0.01, ***p < 0.001.

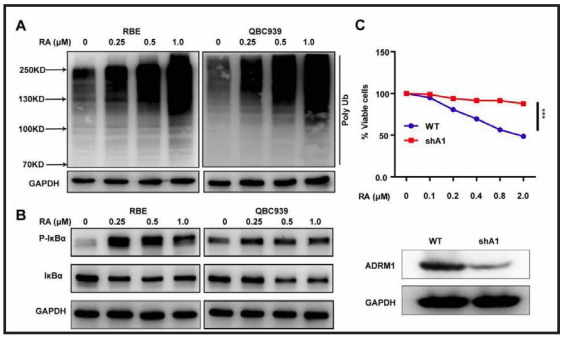

Fig. 4. RA190 inhibited proteasome function through targeting ADRM1. (A) RA190 suppression of the proteasome led to the accumulation of higher-molecular weight polyubiquitylated proteins. After 24 h of treatment, cells were harvested and subjected to immunoblotting. (B) RA190 induced substrate accumulation of ADRM1. (C) QBC939-shA1 and QBC939-WT cells were treated with increasing concentrations of RA190 for 24 h, followed by Cell Counting Kit-8 assay. ***p < 0.001.

that RA190 could impede proteasome function and induce the accumulation of higher-molecular weight polyubiquitylated proteins and phosphorylated IκBα (p-IκBα) in ICC cells. Our results showed that RA190 could induce higher-molecular weight polyubiquitylated protein accumulation in ICC cells (Fig. 4A). We also found that RA190 could induce p-IκBα accumulation in a dose-dependent manner (Fig. 4B). To further determine the specificity of RA190 against ADRM1, we treated QBC939 shA1 and wild-type cells with RA190. Treatment with RA190 triggered a significant decrease in cell viability of wild-type cells (Fig. 4C). These data show that RA190-induced activity is dependent on ADRM1 in ICC cells.

To evaluate the efficacy of RA190 in ICC, we isolated two primary ICC cells (ICC-1 and ICC-2) from two fresh ICC specimens. These primary ICC cells and two ICC cell lines RBE and QBC939 were treated with RA190 for the indicated time. RA190 showed a significant suppressive effect on cell proliferation (Fig. 5A) and clone formation (Fig. 5B) of established ICC cell lines in a dose-dependent manner. By using two primary ICC cells, RA190 also exhibited similar suppressive effect on cell proliferation (Fig.5A) and clone formation (Fig. 5B), in accordance with results from established ICC cell lines. These data demonstrate that inhibition of ADRM1 by RA190 suppresses the proliferation of ICC cells.

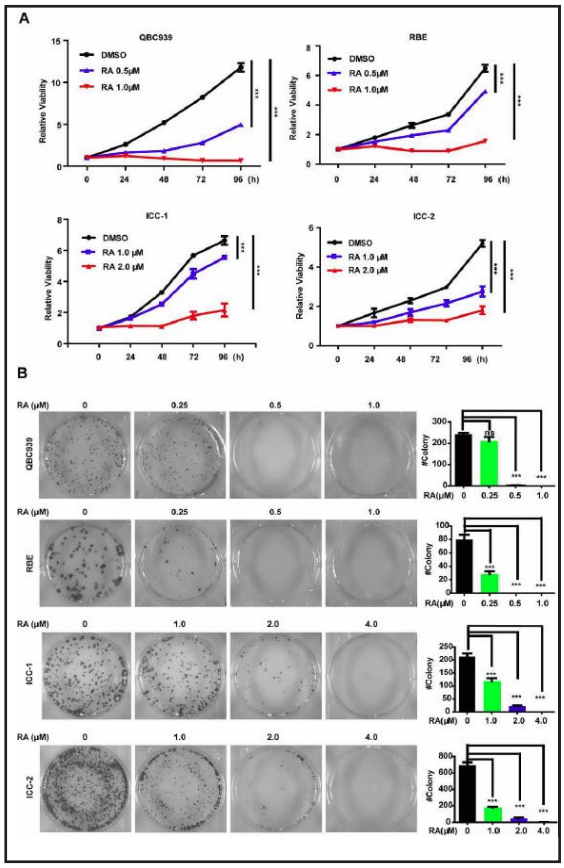

Fig. 5. RA190 suppressed proliferation and colony formation in vitro. (A) RA190 inhibited ICC cell proliferation. Cells were treated with or without RA190 at the indicated doses at the indicated time points, followed by cell counting with the kit-8 assay. (B) RA190 suppressed colony formation of ICC cells. Cells were treated with or without RA190 at the indicated doses for 12 days, followed by crystal violet staining and colony counting. These results are representative of three independent experiments. ***p <0.001, ns, not significant.

RA190 induces G_2-M phase cell cycle arrest and apoptosis of ICC cells

Previous studies demonstrated that ADRM1 was required for proper cell cycle progression [28]. We explored whether RA190 has an effect on the cell cycle of ICC cells. We observed a prominent increase of the G_2-M phase cell population after treatment with RA190 for 24 h (Fig. 6A). After 48 h of treatment with RA190, the sub-G_1 population, representing the apoptosis subgroup [29], was increased significantly (Fig. 6A). When RA190 treatment was performed after cell cycle synchronization by thymidine, the G_2-M phase cell population accumulated significantly in RA190-treated groups (see online suppl. material, Suppl. Fig. 2A). To investigate how RA190 induces G_2-M phase cell cycle arrest, we analyzed cell cycle regulators, including p21 [30], p27 [30, 31] and WEE1 [30, 32], which have been reported to be degraded by the proteasome after ubiquitination [33]. After RA190 treatment, both p21 and WEE1 accumulated significantly, but p27 levels were not affected (see online suppl. material, Suppl. Fig. 2B), indicating that RA190 induces G_2-M phase cell cycle arrest of ICC cells by accumulation of p21 and WEE1.

To determine whether RA190 indeed induces cell apoptosis, we examined the expression of apoptosis markers, cleaved-CASPAS3 and cleaved-PARP [30, 33]. Our results showed that cleaved-CASPAS3 and cleaved-PARP were increased when cells were treated with RA190 (Fig. 6B). Moreover, PUMA, which has a pro-apoptotic role [34], was increased significantly, and γ-H2AX, a DNA damage marker indicating cell apoptosis [30, 33], also accumulated significantly (Fig. 6B). RA190 induction of ICC cell apoptosis was further validated by annexin V/PI double staining assay (Fig. 6C). These data indicate that RA190 induces apoptosis of ICC cells. Taken together, our findings suggest that RA190-induced cell cycle arrest occurs before cell apoptosis in ICC cells.

RA190-induced apoptosis is partially attributed to NF-κB inactivation by p-IκBα accumulation

RA190 can inactivate proteasome function by inhibiting ADRM1. In addition, ADRM1 functions as an adaptor protein regulating degradation of many functional substrates, such as the well-defined NF-κB inhibitor IκBα, [27]. Thus, we hypothesized that the substrates of ADRM1 contributed to RA190-induced cell apoptosis. As shown in Fig. 4B and see online suppl. material, Suppl. Fig 3, p-IκBα accumulated after RA190 treatment in ICC cells.

To determine whether p-IκBα accumulation contributed to RA190-induced apoptosis, we constructed an IκBα knockdown plasmid, and the knockdown efficiency was validated

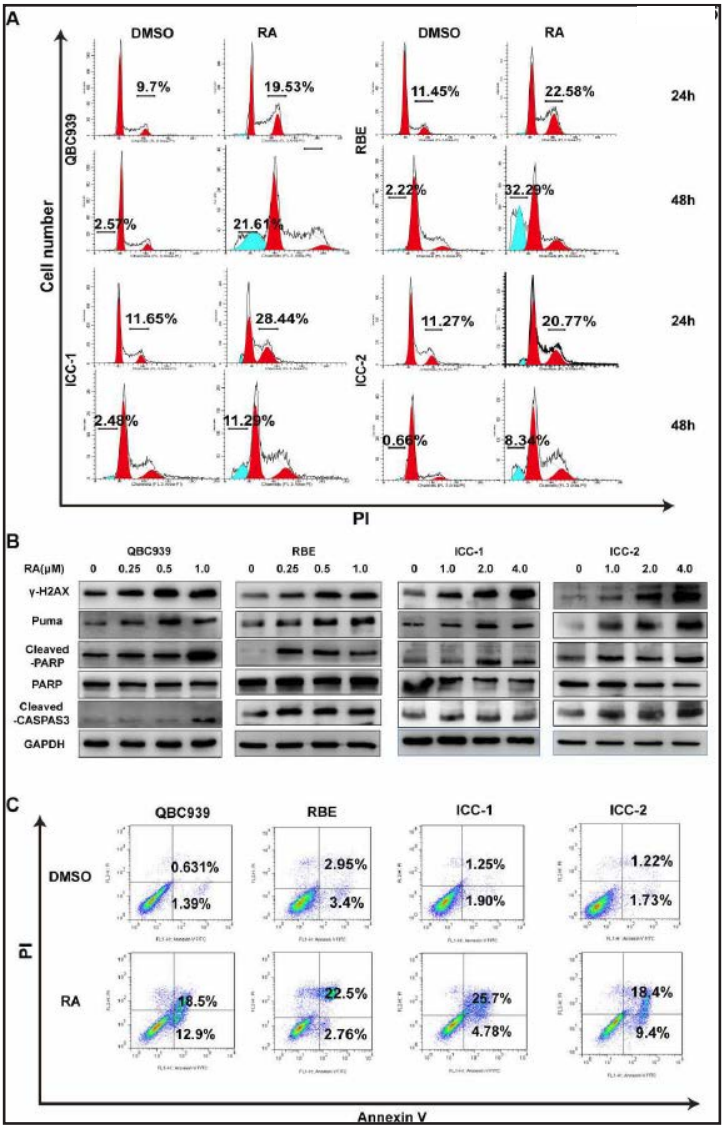

Fig. 6. RA190 induced cell cycle arrest and apoptosis in ICC cells. (A) RA190 induced cell cycle arrest and apoptosis. Cells were harvested and subjected to PI staining and fluorescence-activated cell sorting analysis at the indicated time points. The percentages of cells in the G_2-M and sub-G_1 phases were determined. (B) RA190 induced apoptosis of ICC cells. Cells were harvested and subjected to immunoblotting analysis. (C) Apoptosis in different groups was analyzed by flow cytometry with annexin V/PI. Cells were harvested and subjected to annexin V/PI staining and fluorescence-activated cell sorting analysis. The percentage of apoptotic cells was determined.

by immunoblotting (Fig. 7A). Results indicated that IκBα knockdown decreased the expression of PUMA upon RA190 treatment and attenuated the expression of the apoptosis markers, cleaved-CASPAS3 and cleaved-PARP, compared with the control group (Fig. 7A). Moreover, an apoptosis assay using annexin V/PI double staining further showed that IκBα knockdown attenuated RA190-induced cell apoptosis of ICC cells (Fig. 7B). These data suggest that p-IκBα accumulation is necessary but not sufficient for RA190-induced cell apoptosis.

Inhibition of ADRM1 by RA190 suppresses ICC growth in vivo

To further explore the role of RA190 on ICC growth, we investigated the anti-tumor effect of RA190 *in vivo*. QBC939 cells were injected subcutaneously into nude mice. At the end of RA190 treatment (4 weeks), tumor size and weight were measured (Fig. 8A and 8B). As compared with the control group, tumor size and weight of the RA190-treated group were significantly reduced (Fig. 8A and 8B). No obvious treatment-related adverse effects on body weight, liver function, or kidney function during treatment were observed (see online suppl. material, Suppl. Fig. 4A). These data show that RA190 has promising anti-ICC effects and is well-tolerated *in vivo*.

To further validate the ICC inhibitory mechanism of RA190 *in vivo*, immunohistochemical analyses of proliferation and apoptosis were performed. As expected, increased TUNEL staining was observed in the RA190-treated group compared with the control group (Fig. 8C). Ki-67 staining decreased significantly in RA190-treated group compared with the

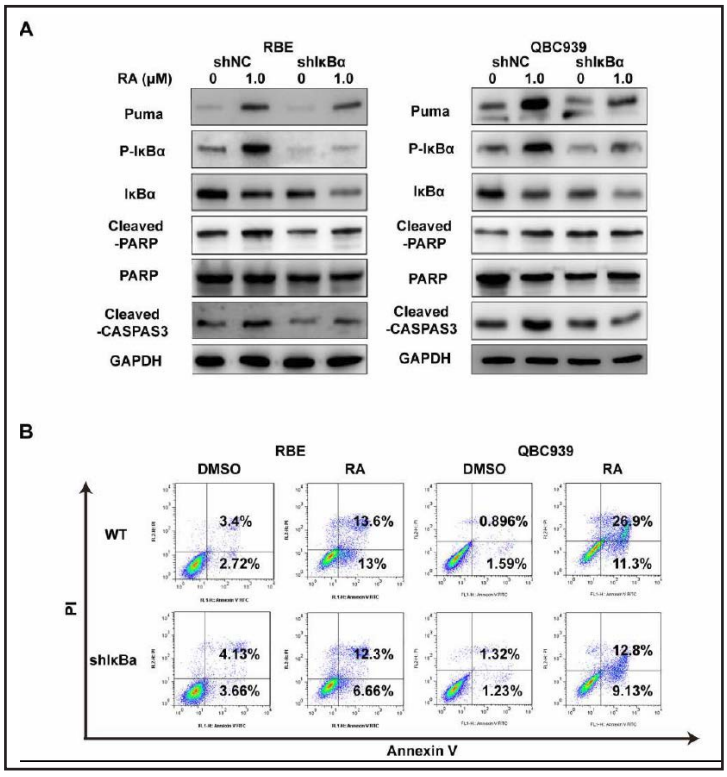

Fig. 7. RA190 induced apoptosis through NF-κb inactivation in ICC cells. (A) Cell apoptosis induced by RA190 was attenuated by IκBα knockdown. RBE and QBC939 cells were transfected with shIκBα and shNC lentivirus to generate RBE shIκBα and QBC939 shIκBα cells. Then cells were treated with or without RA190 for 48 h, harvested and subjected to immunoblotting analysis. (B) Fluorescence-activated cell sorting analysis of cell apoptosis. Cells were harvested and subjected to annexin V/PI staining and fluorescence-activated cell sorting analysis. The percentage of apoptotic cells was determined.

control group, indicating that proliferation was suppressed by RA190 (Fig. 8C). Enhanced p-IκBα and WEE1 staining were observed in RA190-treated tumors, consistent with the *in vitro* expression (Fig. 8C). Finally, we randomly extracted proteins from treated and control tumors to measure the markers of apoptosis, p-IκBα, WEE1 and p21. Consistently, RA190-induced elevated expressions of cleaved-PAPR, cleaved-CASPAS3, and p-IκBα, as well as accumulation of WEE1 and P21, were observed in the RA190-treated group (Fig. 8D). Taken together our data indicate that RA190 has a similar anti-tumor effect and mechanism of action *in vitro* and *in vivo*.

RA190 suppresses tumor growth in an ICC PDX model

We further validated the suppressive effect of RA190 in two PDX mouse models. Consistent with findings from the *in vitro* and subcutaneous mouse model experiments, RA190 showed a powerful suppressive effect on tumor growth in the PDX mouse. Tumor size and weight were reduced by RA190 treatment (Fig. 8A and 8B). Moreover, RA190 treatment was well tolerated (see online suppl. material, Suppl. Fig. 4A).

In the PDX mouse, TUNEL staining was also increased in the RA190-treated group and Ki-67 staining was decreased significantly (Suppl. Fig. 4B). Enhanced staining of p-IκBα and WEE1 were observed in RA190-treated tumors (see online suppl. material, Suppl. Fig. 4B). These data demonstrate that RA190 has a significant anti-tumor effect in the ICC PDX model, consistent with the findings of *in vitro* and subcutaneous mouse model studies.

Discussion

Overexpression of ADRM1 was found in some malignancies [14-18], and high expression of ADRM1 indicated poor prognosis in ovarian cancer [17] and gastric carcinoma [18]. However, to our knowledge, its expression and roles in ICC have not been studied previously. Our results showed that ADRM1 was upregulated at the mRNA and protein levels in ICC tumor tissues. This up-regulation of ADRM1 was correlated with ICC tumor size and indicated

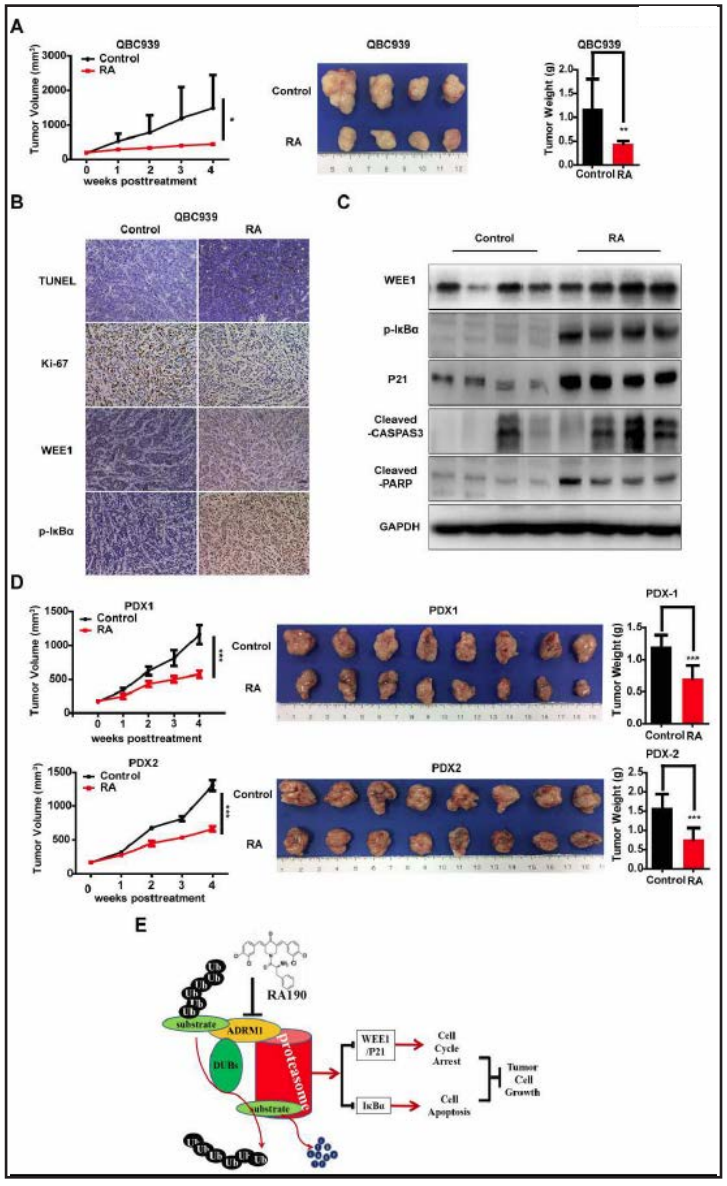

Fig. 8. RA190 suppressed ICC growth in subcutaneous xenograft and PDX models. (A) Subcutaneous xenograft tumors of ICC models were treated with or without RA190 (20 mg/kg) twice a week. Tumor size was determined using calipers once a week. Tumor tissues were harvested, photographed, and weighed. (B) Representative images of immunohistochemical staining of TUNEL, Ki-67, p-IκBα, and WEE1 in xenograft tumors (400 × magnification). (C) Immunoblotting analysis of the indicated markers. Tumors from control and treated groups were selected randomly. (D) Two PDX models were treated with or without RA190 (25 mg/kg) twice a week. Tumor size was determined by caliper measurement once a week. Tumor tissues were harvested, photographed, and weighed. (E) Schematic model; RA190 induced cell cycle arrest and apoptosis to suppress ICC cell growth through the accumulation of proteasome substrates in vitro and in vivo. *p<0.05, **p<0.01, ***p < 0.001.

a shorter RFS and OS in ICC patients. ADRM1 overexpression also predicted a poor prognosis in liver, lung cancer, and renal cancers and glioblastoma according to TCGA dataset. These findings suggest that ADRM1 has a pathogenetic role in cancer and may serve as a potential anti-cancer target in ICC.

Targeting ADRM1 by RNA interference significantly suppressed ICC cell proliferation both *in vivo* and *in vitro*. These data are consistent with some early studies showing that ADRM1 knockdown suppressed cell proliferation in hepatocellular carcinoma [15] and ovarian cancer [16]. These results imply that targeting ADRM1 is a promising strategy to treat cancers. However, there is no drug targeting ADRM1 in clinical use.

Recently, a small molecule targeting ADRM1 was developed. RA190, which can covalently bind to cysteine 88 of ADRM1 in the 19S regulatory particle of proteasome, inhibits proteasome function, resulting in higher-molecular weight polyubiquitylated protein accumulation [14, 19]. In HCT116 cells, RA190 can also bind with UCH37, a de-ubiquitinating enzyme interacting with ADRM1, to suppress proteasome function [35]. Meanwhile, it was reported that KDT-11 could also suppress multiple myeloma by targeting ADRM1 [36]. In ICC cells the specificity of RA190 on ADRM1 inhibition was confirmed by :

(1) the accumulation of higher-molecular weight polyubiquitylated proteins and p-IκBα in RA190-treated ICC cells; and (2) reduced RA190 sensitivity following knockdown of ADRM1 in ICC cells [14].

Previous studies showed that RA190 can suppress cancer cell growth and induce cell apoptosis in multiple myeloma [14, 19] and ovarian carcinoma [19], and can overcome bortezomib resistance in multiple myeloma [14, 19]. In the present study, we found that RA190 significantly suppressed cell proliferation and colony formation in both established ICC cell lines and primary ICC cells, and targeting ADRM1 by RA190 in these ICC cells could induce G_2-M phase cell cycle arrest and the accumulation of WEE1 and p21, which was similar to previous findings [28].

Cancer cells have a tendency to escape cell apoptosis by inactivating apoptosis signal pathways through down-regulating pro-apoptotic proteins or up-regulating anti-apoptotic proteins. Thus, induction of cell apoptosis was an exportable anti-tumor strategy in cancer therapy [37, 38]. We noted that targeting ADRM1 by RA190 induced cell apoptosis of multiple myeloma [14, 19], but the mechanism remains unclear. It was also reported that RA190 induced cell apoptosis by triggering endoplasmic reticulum stress and resulted in an unresolved unfolded protein response [19]. In the present study, we found that targeting ADRM1 induced ICC cell apoptosis through increasing PUMA expression by inducing p-IκBα accumulation. IκBα is a substrate of ADRM1, and a key inhibitor of the NF-κB signaling pathway [27]. The NF-κB pathway is constitutively active in a variety of human cancers including ICC [39]. Abolishing NF-κB activation by curcumin or caffeic acid phenethyl ester suppressed ICC cell growth by inducing apoptosis [39, 40]. It was reported also that AKT/NF-κB activation suppressed PUMA expression by up-regulating Slung upon fragile histidine triad loss in non-small cell lung cancer [41]. Moreover, PUMA, a downstream gene of p53[42], was directly regulated by TNF-α through activating NF-κB [43]. We found that the NF-κB signaling pathway was suppressed by p-IκBα accumulation upon RA190 treatment and PUMA was up-regulated resulting in cell apoptosis. However, levels of p53 and p-p53 (s15) were not affected by RA190 (data not shown). Nevertheless, the mechanism of action was not considered in this study. Also, IκBα knockdown only partially rescued RA190-induced cell apoptosis and PUMA accumulation. It is possible that there are other signaling pathways involved in RA190-induced cell apoptosis, and further investigations are needed to understand the relationship between NF-κB signaling pathway and PUMA upon targeting ADRM1 and the signaling pathways involved in targeting ADRM1-induced cell apoptosis.

Recently, the PDX mouse model has been used to identify personalized therapy for cancer patients [44]. In our study, a subcutaneously transplanted tumor model of ICC and two PDX mouse models demonstrated the anti-tumor effects of RA190 *in vivo*. Consistent with its effects *in vitro*, RA190 suppressed transplanted tumor growth significantly. Our analysis revealed that RA190 induced apoptosis in treated tumors, suggesting that the mechanisms of action of RA190 are similar *in vitro* and *in vivo*. Notably, RA190-treated mice showed good tolerance during the entire treatment period. In fact, another proteasome inhibitor, bortezomib, was approved by the FDA. However, since bortezomib suppresses the degradation of all substrates in the proteasome system, it is highly toxic [45]. RA190 only blocks the degradation of specific substrates regulated by ADRM1. This selectively might provide a high degree of safety of RA190 for clinical application [14, 19, 28].

Conclusion

In summary, this is the first report that ADRM1 was overexpressed in ICC both at the mRNA and protein levels, and overexpression of ADRM1 was associated with tumor size and predicted poor prognosis in ICC. Based on both *in vitro* and *in vivo* investigations, including in established cell lines, primary ICC cells, and subcutaneously transplanted tumor and PDX models, we showed that RA190 suppressed ICC cell growth by inducing G_2-M phase cell cycle arrest and NF-κB-regulated cell apoptosis (Fig 8E). These findings indicate that ADRM1 may

provide a promising target for ICC treatment and support the clinical investigation of ADRM1 inhibitors (e.g., RA190 and KDT-11) for ICC treatment in the future.

Acknowledgements

This research was supported by the "973" State Key Basic Research Program of China (2013CB910500, L.X.Q), China National Natural Science Foundation (81672820, L.X.Q), China National Key Projects for Infectious Disease (2012ZX10002-012, L.X.Q), and the National Key Research and Development Program of China (2017 YFC 1308604, Q.Z.D).

Disclosure Statement

The authors declare that they have no competing interests.

References

1 Sia D, Losic B, Moeini A, Cabellos L, Hao K, Revill K, Bonal D, Miltiadous O, Zhang Z, Hoshida Y: Massive parallel sequencing uncovers actionable FGFR2–PPHLN1 fusion and ARAF mutations in intrahepatic cholangiocarcinoma. Nat Commun 2015;6: 6087.
2 Rizvi S, Gores GJ: Pathogenesis, diagnosis, and management of cholangiocarcinoma. Gastroenterology 2013;145:1215-1229.
3 Gao Q, Yu G-Y, Shi J-Y, Li L-H, Zhang W-J, Wang Z-C, Yang L-X, Duan M, Zhao H, Wang X-Y: Neddylation pathway is up-regulated in human intrahepatic cholangiocarcinoma and serves as a potential therapeutic target. Oncotarget 2014;5:7820.
4 Lu X, Zhou C, Li R, Deng Y, Zhao L, Zhai W: Long Noncoding RNA AFAP1-AS1 Promoted Tumor Growth and Invasion in Cholangiocarcinoma. Cell Physiol Biochem 2017;42:222-230.
5 Razumilava N, Gores GJ: Cholangiocarcinoma. Lancet 2014;383:2168-2179.
6 Bridgewater J, Galle PR, Khan SA, Llovet JM, Park J-W, Patel T, Pawlik TM, Gores GJ: Guidelines for the diagnosis and management of intrahepatic cholangiocarcinoma. J hepatol 2014;60:1268-1289.
7 Sia D, Tovar V, Moeini A, Llovet J: Intrahepatic cholangiocarcinoma: pathogenesis and rationale for molecular therapies. Oncogene 2013;32:4861-4870.
8 Collins GA, Goldberg AL: The Logic of the 26S Proteasome. Cell 2017;169:792-806.
9 Bedford L, Lowe J, Dick LR, Mayer RJ, Brownell JE: Ubiquitin-like protein conjugation and the ubiquitin–proteasome system as drug targets. Nat Rev Drug Discov 2011;10:29-46.
10 Dobbelstein M, Moll U: Targeting tumour-supportive cellular machineries in anticancer drug development. Nat Rev Drug Discov 2014;13:179-196.
11 Liu R, Fu C, Sun J, Wang X, Geng S, Zou J, Bi Z, Yang C: A New Perspective for Osteosarcoma Therapy: Proteasome Inhibition by MLN9708/2238 Successfully Induces Apoptosis and Cell Cycle Arrest and Attenuates the Invasion Ability of Osteosarcoma Cells in vitro. Cell Physiol Biochem 2017;41:451-465.
12 Weathington NM, Mallampalli RK: Emerging therapies targeting the ubiquitin proteasome system in cancer. J Clin Invest 2014;124:6-12.
13 Yao T, Song L, Xu W, DeMartino GN, Florens L, Swanson SK, Washburn MP, Conaway RC, Conaway JW, Cohen RE: Proteasome recruitment and activation of the Uch37 deubiquitinating enzyme by Adrm1 Nat Cell Biol 2006;8:994-1002.
14 Song Y, Ray A, Li S, Das D, Tai Y, Carrasco R, Chauhan D, Anderson K: Targeting proteasome ubiquitin receptor Rpn13 in multiple myeloma. Leukemia 2016;30:1877-1886.
15 Yang X, Miao X, Wen Y, Hu J, Dai W, Yin B: A possible connection between adhesion regulating molecule 1 overexpression and nuclear factor kappa B activity in hepatocarcinogenesis. Oncol Rep 2012;28:283.
16 Fejzo MS, Anderson L, Von Euw EM, Kalous O, Avliyakulov NK, Haykinson MJ, Konecny GE, Finn RS, Slamon DJ: Amplification target ADRM1: role as an oncogene and therapeutic target for ovarian cancer. Int J Mol Sci 2013;14:3094-3109.

17 Fejzo MS, Dering J, Ginther C, Anderson L, Ramos L, Walsh C, Karlan B, Slamon DJ: Comprehensive analysis of 20q13 genes in ovarian cancer identifies ADRM1 as amplification target. Gene Chromosome Canc 2008;47:873-883.
18 Jang SH, Park JW, Kim HR, Seong JK, Kim HK: ADRM1 gene amplification is a candidate driver for metastatic gastric cancers. Clin Exp Metastasis 2014;31:727-733.
19 Anchoori RK, Karanam B, Peng S, Wang JW, Jiang R, Tanno T, Orlowski RZ, Matsui W, Zhao M, Rudek MA: A bis-benzylidine piperidone targeting proteasome ubiquitin receptor RPN13/ADRM1 as a therapy for cancer. Cancer Cell 2013;24:791-805.
20 Tian J, Tang ZY, Ye S, Liu Y, Lin Z, Chen J, Xue Q: New human hepatocellular carcinoma (HCC) cell line with highly metastatic potential (MHCC97) and its expressions of the factors associated with metastasis. Brit J Cancer 1999;81:814.
21 Chen P, Hu T, Liang Y, Li P, Chen X, Zhang J, Ma Y, Hao Q, Wang J, Zhang P: Neddylation Inhibition Activates the Extrinsic Apoptosis Pathway through ATF4–CHOP–DR5 Axis in Human Esophageal Cancer Cells. Clin Cancer Res 2016;22:4145-4157.
22 Andersen JB, Spee B, Blechacz BR, Avital I, Komuta M, Barbour A, Conner EA, Gillen MC, Roskams T, Roberts LR: Genomic and genetic characterization of cholangiocarcinoma identifies therapeutic targets for tyrosine kinase inhibitors. Gastroenterology 2012;142:1021-1031, e1015.
23 Spagnuolo P, Hurren R, Gronda M, MacLean N, Datti A, Basheer A, Lin F, Wang X, Wrana J, Schimmer A: Inhibition of intracellular dipeptidyl peptidases 8 and 9 enhances parthenolide's anti-leukemic activity. Leukemia 2013;27:1236.
24 Song W, Hwang Y, Youngblood V, Cook R, Balko J, Chen J, Brantley-Sieders D: Targeting EphA2 impairs cell cycle progression and growth of basal-like/triple-negative breast cancers. Oncogene 2017; 36(40): 5620.
25 Ho C-H, Tsai S-F: Functional and biochemical characterization of a T cell-associated anti-apoptotic protein, GIMAP6. J Biol Chem 2017;292:9305-9319.
26 Morton CL, Houghton PJ: Establishment of human tumor xenografts in immunodeficient mice. Nat Protoc 2007;2:247-250.
27 Mazumdar T, Gorgun FM, Sha Y, Tyryshkin A, Zeng S, Hartmann-Petersen R, Jørgensen JP, Hendil KB, Eissa NT: Regulation of NF-κB activity and inducible nitric oxide synthase by regulatory particle non-ATPase subunit 13 (Rpn13). Proc Natl Acad Sci USA 2010;107:13854-13859.
28 Randles L, Anchoori RK, Roden RB, Walters KJ: The Proteasome Ubiquitin Receptor hRpn13 and Its Interacting Deubiquitinating Enzyme Uch37 Are Required for Proper Cell Cycle Progression. J Biol Chem 2016;291:8773-8783.
29 Yun U-J, Sung JY, Park S-Y, Ye S-K, Shim J, Lee J-S, Hibi M, Bae Y-K, Kim Y-N: Oncogenic role of rab escort protein 1 through EGFR and STAT3 pathway. Cell Death Dis 2017;8:e2621.
30 Luo Z, Yu G, Lee HW, Li L, Wang L, Yang D, Pan Y, Ding C, Qian J, Wu L, Chu Y, Yi J, Wang X, Sun Y, Jeong LS, Liu J, Jia L: The Nedd8-activating enzyme inhibitor MLN4924 induces autophagy and apoptosis to suppress liver cancer cell growth. Cancer Res 2012;72:3360-3371.
31 Wan C, Hou S, Ni R, Lv L, Ding Z, Huang X, Hang Q, He S, Wang Y, Cheng C, Gu XX, Xu G, Shen A: MIF4G domain containing protein regulates cell cycle and hepatic carcinogenesis by antagonizing CDK2-dependent p27 stability. Oncogene 2015;34:237-245.
32 Ma H, Takahashi A, Sejimo Y, Adachi A, Kubo N, Isono M, Yoshida Y, Kanai T, Ohno T, Nakano T: Targeting of Carbon Ion-Induced G2 Checkpoint Activation in Lung Cancer Cells Using Wee-1 Inhibitor MK-1775 Radiat Res 2015;184:660-669.
33 Li L, Wang M, Yu G, Chen P, Li H, Wei D, Zhu J, Xie L, Jia H, Shi J, Li C, Yao W, Wang Y, Gao Q, Jeong LS, Lee HW, Yu J, Hu F, Mei J, Wang P, Chu Y, Qi H, Yang M, Dong Z, Sun Y, Hoffman RM, Jia L: Overactivated neddylation pathway as a therapeutic target in lung cancer. J Natl Cancer Inst 2014;106:dju083.
34 Glab JA, Doerflinger M, Nedeva C, Jose I, Mbogo GW, Paton JC, Paton AW, Kueh AJ, Herold MJ, Huang DC: DR5 and caspase-8 are dispensable in ER stress-induced apoptosis. Cell Death Differ 2017; 24(5): 944.
35 Lu X, Nowicka U, Sridharan V, Liu F, Randles L, Hymel D, Dyba M, Tarasov SG, Tarasova NI, Zhao XZ: Structure of the Rpn13-Rpn2 complex provides insights for Rpn13 and Uch37 as anticancer targets. Nat Commun 2017;8:ncomms15540.
36 Trader DJ, Simanski S, Kodadek T: A reversible and highly selective inhibitor of the proteasomal ubiquitin receptor rpn13 is toxic to multiple myeloma cells. J Am Chem Soc 2015;137:6312-6319.

37 Jia L, Yang J, Hao X, Zheng M, He H, Xiong X, Xu L, Sun Y: Validation of SAG/RBX2/ROC2 E3 ubiquitin ligase as an anticancer and radiosensitizing target. Clin Cancer Res 2010;16:814-824.
38 Gan PP, Zhou YY, Zhong MZ, Peng Y, Li L, Li JH: Endoplasmic Reticulum Stress Promotes Autophagy and Apoptosis and Reduces Chemotherapy Resistance in Mutant p53 Lung Cancer Cells. Cell Physiol Biochem 2017;44:133-151.
39 Prakobwong S, Gupta SC, Kim JH, Sung B, Pinlaor P, Hiraku Y, Wongkham S, Sripa B, Pinlaor S, Aggarwal BB: Curcumin suppresses proliferation and induces apoptosis in human biliary cancer cells through modulation of multiple cell signaling pathways. Carcinogenesis 2011;32:1372-1380.
40 Onori P, DeMorrow S, Gaudio E, Franchitto A, Mancinelli R, Venter J, Kopriva S, Ueno Y, Alvaro D, Savage J: Caffeic acid phenethyl ester decreases cholangiocarcinoma growth by inhibition of NF-κB and induction of apoptosis. Int J Cancer 2009;125:565-576.
41 Wu DW, Lee MC, Hsu NY, Wu TC, Wu JY, Wang YC, Cheng YW, Chen CY, Lee H: FHIT loss confers cisplatin resistance in lung cancer via the AKT/NF-kappaB/Slug-mediated PUMA reduction. Oncogene 2015;34:3882-3883.
42 Nakano K, Vousden KH: PUMA, a novel proapoptotic gene, is induced by p53. Mol Cell 2001;7:683-694.
43 Wang P, Qiu W, Dudgeon C, Liu H, Huang C, Zambetti GP, Yu J, Zhang L: PUMA is directly activated by NF-kappaB and contributes to TNF-alpha-induced apoptosis. Cell Death Differ 2009;16:1192-1202.
44 Bondarenko G, Ugolkov A, Rohan S, Kulesza P, Dubrovskyi O, Gursel D, Mathews J, O'Halloran TV, Wei JJ, Mazar AP: Patient-derived tumor xenografts are susceptible to formation of human lymphocytic tumors. Neoplasia 2015;17:735-741.
45 Manasanch EE, Orlowski RZ: Proteasome inhibitors in cancer therapy. Nat Rev Clin Oncol 2017;14: 417.